Di- and heptavalent nicotinic analogues to interfere with alpha 7 nicotinic acetylcholine receptors

Yoan Brissonnet, Rómulo Aráoz, Rui Sousa, Lucie Percevault, Sami Brument, David Deniaud, Denis Servent, Jean-Yves Le Questel, Jacques Lebreton, Sebastien G. Gouin

Di- and heptavalent nicotinic analogues to interfere with α7 nicotinic acetylcholine receptors

Yoan Brissonnet,[a] Romulo Araoz,[b,c *] Rui Sousa,[a] Lucie Percevault,[a] Sami Brument,[a] David Deniaud,[a] Denis Servent,[c] Jean-Yves Le Questel,[a*] Jacques Lebreton, [a] Sébastien G. Gouin[a*]

[a] *Université de Nantes, CEISAM, Chimie Et Interdisciplinarité, Synthèse, Analyse, Modélisation, UMR CNRS 6230, UFR des Sciences et des Techniques, 2, rue de la Houssinière, BP 92208, 44322 Nantes Cedex 3, France.*
[b] *CNRS, Neuro-PSI, UMR9197, 91191 Gif sur Yvette, France*
[c] *CEA/DRF/ JOLIOT/SIMOPRO/ Toxines Récepteur et Canaux Ioniques, F-91191, Gif-Sur-Yvette, France*

ARTICLE INFO

Keywords:
Multivalency
Nicotinic acetylcholine receptors
Multivalent nicotinics

ABSTRACT

In the field of nicotinic acetylcholine receptors (nAChRs), recognized as important therapeutic targets, much effort has been dedicated to the development of nicotinic analogues to agonize or antagonize distinct homo- and heteropentamers nAChR subtypes, selectively. In this work we developed di- and heptavalent nicotinic derivatives based on ethylene glycol (EG) and cyclodextrin cores, respectively. The compounds showed a concentration dependent inhibition of acetylcholine-induced currents on α7 nAChR expressed by Xenopus oocytes. Interesting features were observed with the divalent nicotinic derivatives, acting as antagonists with varied inhibitory concentrations (IC_{50}) in function of the spacer arm length. The best divalent compounds showed a 16-fold lowered IC_{50} compared to the monovalent reference (12 vs 195 μM). Docking investigations provide guidelines to rationalize these experimental findings.

1. Introduction

Synthetic multivalent systems, bearing several copies of a given ligand, have been widely developed to interfere with multimeric proteins. Affinity enhancements of several orders of magnitudes can be reached when the multivalent ligands span across the different recognition domains of the receptor. These chelate interactions are distinct from positive cooperativity or allosteric controls. They are driven by high local concentrations of the cognate ligands when the first is bound and by the lower entropic costs paid due to ligand preorganization at the protein surface. Most of the successful examples are so far reported with synthetic glycoclusters targeting carbohydrate binding proteins (lectins),[1,2] which are particularly prone to multivalent interactions due to their generally multimeric nature and shallow binding domains. Recently, the concept of multivalency has been extended to carbohydrate processing enzymes such as glycosidases and glycosyltransferases.[3–7] The multivalent effects were studied and ascribed to different binding modes such as interactions in secondary subsites,[8,9] in additional carbohydrate binding modules,[10] and the formation of stabilized cross-linked aggregates.[11,12]
Although mostly exemplified in the field of glycosciences,[13,14] multivalent ligands were also reported for proteins and enzymes involved in cellular signal transduction pathways.[15–17] Strong increased affinity were reported with homo and heterobivalent ligands of members of the G-protein coupled receptors (GPCRs) including the oxytocin receptor, [18] muscarinic acetylcholine receptor,[19] and γ-aminobutyric acid type A receptors.[20]
Kramer and Karpen have designed dimeric agonists of cyclic-nucleotide-gated channels (CNG) allowing ions to flow across cell membranes for signal transduction in retinal photoreceptors and olfactory neurons.[21] Cyclic guanosyl monophosphate (cGMP) was linked through polyethyleneglycols spacers (PEGs) of different lengths. Divalent cGMP with optimal PEG lengths to match the distance between the CNG binding sites were shown to be up to a thousand times more potent activators than monovalent cGMP. More recently, Capelli and coworkers designed dendrimeric tetravalent ligands with picomolar affinity for the serotonin-gated ion channel 5-HT_3.[22]
Altogether these results highlight the benefits of targeting ligand-gated ion channels (LGIC) in their orthosteric and/or allosteric binding sites with multivalent ligands.
Nicotinic acetylcholine receptors (nAChRs) are important members of the LGIC superfamily, involved in cellular signalling of the peripheral and central nervous system. Agonists or antagonists of neuronal nAChRs have been extensively developed as analgesic targets or as potential drugs to treat neurological disorders such as schizophrenia, depression and Alzheimer's disease.[23–25] The main difficulty in this approach is to develop selective drugs to target the pharmacologically distinct homo- and heteropentamer nAChR subtypes resulting from the assembly of diverse subunits (α1-α10, β1–β4, γ, δ, ε). The heterogeneity of nAChR subtypes and subunits greatly complicates the design of potent monovalent agonists and antagonists with selective profiles. Acetylcholine binding proteins (AChBP)

are valuable structural surrogates of the extracellular domain of α7 nAChRs albeit their low sequence identity to nAChRs.[26] A systematic modification of the sequence of AChBP toward a closer sequence identity with the homomeric human α7 nAChR was conducted by Taylor and Nemecz and the corresponding structured chimeric proteins have been shown to resemble the binding characteristics of the native receptor.[27] From a structural point of view, the crystallographic structure of the complex between methyllycaconitine and one α7/*Ac*-AChBP (3SIO pdb entry) may therefore be used as a relevant model to investigate the interactions of antagonists to α7 nAChR. In the same vein, an α7–AChBP chimera was designed by Lin Chen and coworkers and X-ray crystal structures of the resulting pentamer and its complex with epibatidine (PDB code 3SQ6), an efficient agonist, were determined.[28] These crystallographic structures can therefore be used as useful templates in the design of α7 nAChRs selective drugs and the study of the behavior of ligands of special interest.

The aim of this study is to assess if multivalent nicotinic derivatives could function as modulators of the nAChRs. Although the concept has previously been evoked,[29] there has been, to our knowledge, no report of such multivalent ligands in the literature. The binding properties of mono- and multivalent nicotinic derivatives **1**-**8** were investigated on α7 nAChRs. The α7 nAChR subtype is a major neuronal receptor, abundantly present in the hippocampus and prefrontal cortex. It forms homopentameric structures displaying five potential nicotinic binding sites at the α subunits interfaces.[24,30] In the present work, the α7/*Ac*-AChBP x-ray structure (3SIO pdb entry) has been used for a preliminary molecular modeling investigation of the binding characteristics of some nicotinic derivatives (**1**, **2** and **3**) in a first attempt to rationalize some of the experimental observations.

2. Results and Discussion

To simplify the chemical synthesis, the multivalent nicotinic analogues were designed racemic, from the monovalent nicotinic synthon altinicline (SIB-1508Y) that reached phase II for the treatment of Parkinson's disease. Its racemic synthesis is relatively straightforward, and the R,S enantiomers were shown to agonize multimeric neuronal nAChR bearing a β-subunit.[31] Preliminary results showed the SIB-1508Y behaved as an antagonist of α7 nAChR. This observation, together with the fact that α7 nAChRs are homopentameric, possessing five ACh-binding sites, allowed us to use this receptor as a model for our study of mutivalent altinicline compounds. The presence of a triple bond also offered the opportunity of a direct grafting to azide-armed scaffolds by copper-catalyzed azide-alkyne cycloaddition (CuAAC). A monovalent (**1**) and five divalent (**2**-**6**) compounds were designed from ethylene glycol (EG) cores of different lengths. EGs were selected for their high flexibility, hydrophilicity and because they do not interact non-specifically with proteins.[32] Indeed, EG conserve a conformational mobility even when the attached ligand is bound to the protein,[33] allowing the second ligand to reach a secondary binding sites. An heptavalent nicotinic **8** and its monovalent analogue **7** were also obtained from mono- and heptazido-β-cyclodextrins, a scaffold that we previously reported to design multivalent *E.coli* antiadhesives that prove effective *in vitro* and *in vivo*.[34]

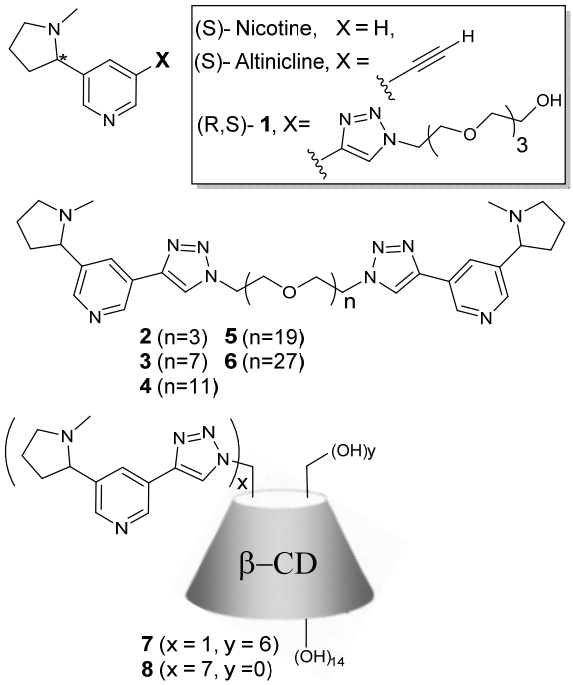

Figure 1. Structure of (S)-nicotine, altinicline and the racemic mono- (**1**, **7**), di- (**2**-**6**) and heptavalent (**8**) nicotinic analogues.

We suggest that a chelate interaction between nAChRs and the multivalent nicotinic design would not be favoured (Figure 2A). The various structural data available at the atomic resolution from molluscean AChBP for example, *Lymnaea stagnalis*,[26] have shown that the nicotinic binding sites are buried from the solvent at the protomers interface.[35] As a consequence, a chelate interaction with a divalent nicotinic analog would require linkers embracing a high distance, of around 80Å. We roughly estimated that the required EG units to span this distance would be of 18 when considering the extended EG conformation. Compounds **5** and **6** designed in the present study would fit with this requirement. However, it was previously shown that the average PEG length in solution, which is proportional to the root mean square of the PEG molecular weight, is much shorter than the extended conformation and more representative of the effective PEG length.[36] For example, Kramer and Karpen found that a 2000 PEG (44 EG unit) was optimum for a divalent cGMP to activate binding sites of CNG channels separated by 39Å.[21]

Instead of potentially targeting the receptor in a chelate fashion, we foresee that compounds **2**-**6** and **8** may interact with α7 nAChRs by other binding mechanisms previously observed with different classes of proteins. This includes the rebinding processes where the tethered ligands can "bind and jump" in a single site due to their high effective concentration (Figure 2C),[37] the interaction in both orthosteric and lower affinity peripheral sites simultaneously by a heterochelate-type interaction (Figure 2B),[16] and the formation of stabilized cross-linked receptors at the membrane surface (Figure 2D).[38]

The alcohol group of commercially available EGs were first activated in O-mesylate group with methanesulfonyl chloride and triethylamine.[39] After substitution using sodium azide in DMF, the corresponding functionalized EGs **9**-**14** were obtained with good yields.[40]

Racemic altinicline was obtained in nine steps from bromonicotinic acid, by a procedure previously described by Cosford and co-workers.[31] This protocol was reproducible, allowing the obtention of gram quantities of altinicline. The triple bond of the ligand was used as an anchor for its grafting to the azido-functionalized linkers **9**-**14** and to the β-cyclodextrin scaffolds **15**[41] and **16**[42] by a CuAAC protocol (Scheme 1).

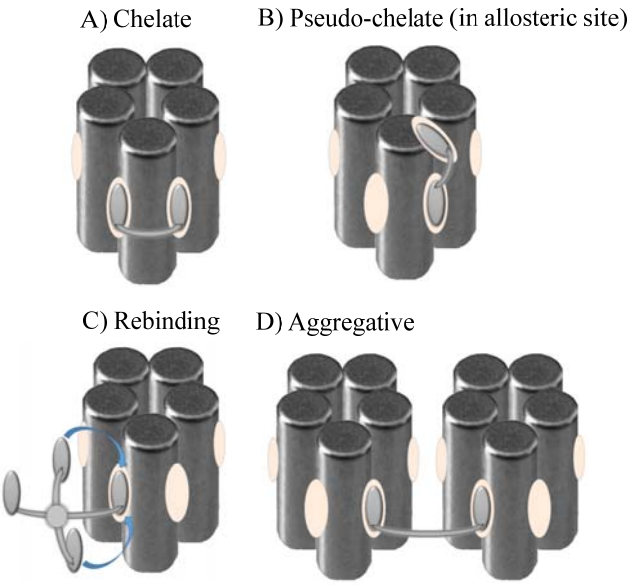

Figure 2. Potential binding modes between di or tetravalent ligands and pentameric nAChRs. A) Chelate binding mode at two protomers interfaces; B) Binding of the cognate nicotinic ligand in a subsite located in proximity of the primary binding domain; C) effects of the high ligands concentration favouring a rebinding process; D) Formation of cross-linked aggregates at the membrane surface.

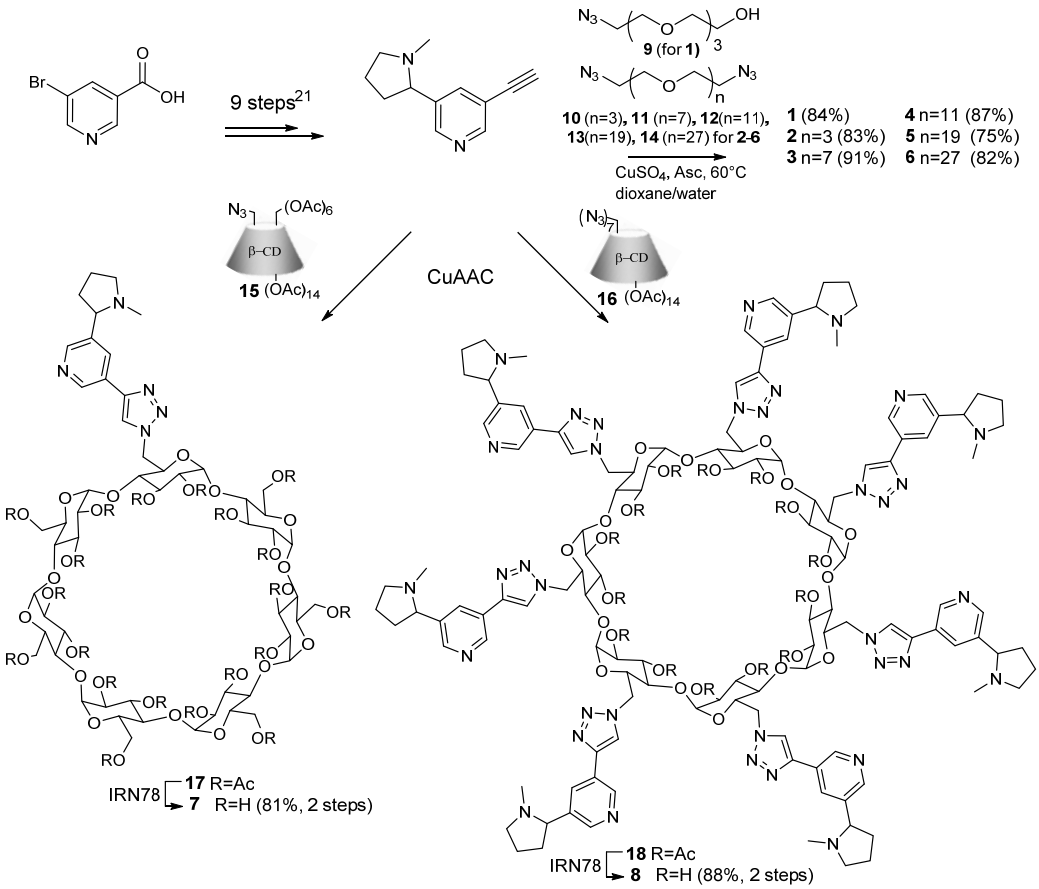

Scheme 1. Synthesis of the nicotinic derivatives **1**-**8**

The compounds were dissolved in dioxane and water with sodium ascorbate and copper sulfate as catalysts. After a night at 60°C, the mono- (**1** and **17**), di- (**2**-**6**), and heptavalent (**18**) compounds were obtained with high

yields. As generally observed with CuAAC, 1,2,3-triazol 1,4-regioisomers were formed in all cases as evidenced by the large Δ(δC-4–δC-5) values (>20 ppm) observed by ^{13}C NMR.[43] Prior to chromatography purification, the crude mixtures were washed with an EDTA solution in order to avoid copper contamination. The acetate groups of compounds **17** and **18** were deprotected on a basic resin (IRN78) to give **7** an **8**. Finally, the compounds were purified by size-exclusion chromatography.

Biological assay

Nicotinic agonists and antagonists can compete for binding the orthosteric site located at the extracellular domain of the nAChR. It should be noted that subtle structural modifications of a given ligand can dramatically impact its selectivity profile for nAChR subtypes and the nature of the current response. In contrast to nicotine (Figure 1, X=H) which is the natural agonist of human α7 receptor, altinicline (X= -C≡CH) did not elicit inwards currents in *Xenopus oocytes* expressing α7.[31] Thus, the oocyte was exposed to ACh at its EC_{50} concentration (100 μM) for three times spaced by 4 min washing with buffer, afterwards, the oocytes were incubated for 1 min to a given concentration of a given multivalent compound and immediately shifted to a well containing a mixture of 100 μM ACh and the multivalent compound at the same concentration. The exposure of oocytes expressing α7 nAChRs did not elicite any changes at the oocyte membrane potential, however, when exposed to the mixture ACh-multivalent compounds, the evoked ACh-inward current was reduced when compared to the ACh-control currents obtained at the beginning of each experiment. The multivalent nicotinic ligands showed a concentration dependent inhibition of ACh-induced currents on α7 nAChRs expressed by Xenopus oocytes. Here, the introduction of a triazol moiety formed during CuAAc leads to compounds with an electrophysiological response that may significantly differ between nicotine and SIB-15087. Thus, to quantify a multivalent effect, it is more relevant to compare multivalent **2**-**6** and **8** with their monovalent analogues **1** and **7**, respectively, than with nicotine or SIB-15087 that do not carry the triazol ring. Compounds **1**-**8** were all shown to exert antagonist effects on human α7 nAChRs with inhibition constants ranging from 12 to 611 μM (Table 1).

The multivalent effects were quantified by dividing the IC_{50} value of the compound by the IC_{50} of the corresponding monovalent reference (i.e.; **1** for **2**-**6** and **7** for **8**). This relative potency number (Rp) was further corrected (divided) by the valency of the compound to lead to the relative inhibitory potency (RIP) factor representing the enhancement per nicotinic ligand (Table 1). Most of the compounds showed negative multivalent effects with RIP values < 1. However, we were pleased to see that positive multivalent effects were observed for divalent compounds **2** and **6**, which are respectively 16 (RIP = 8) and 9 (RIP = 4.6) fold more potent than reference **1**. These two compounds likely interact with their target by different binding modes as their spacer arm length differs significantly in size and because compounds **3**-**5** of intermediate EG numbers showed β values<1. Rebinding mechanisms (Figure 1A) or additional interactions in close binding site proximity (Figure 1B) may prevail for compounds **2** bearing short spacers. Interestingly, a gradual extension of the EG numbers (n = 7→11→19→27) leads to a gradual decrease of the IC_{50} values (611→300→160→21 μM). Similar evolutions of the affinity or inhibitory constants in function of EG length were previously reported with multivalent ligands bearing shorter EG spacers than required to bridge protein binding domains.[21,36] This suggests that bivalent compounds with higher numbers of EG units may perform better in terms of antagonists.

Table 1. Inhibition Constants for ligands **1**-**8** on ACh-Evoked Nicotinic Currents in Xenopus Oocytes

Cpds	Val	IC_{50} (μM)[a]	RIP
1 (n=3 ref)	1	195 (86 – 442)	1
2 (n=3)	2	12 (7 – 20)	8.1
3 (n=7)	2	611 (130 – 2876)	0.16
4 (n=11)	2	300 (156 – 578)	0.32
5 (n=19)	2	160 (88 – 291)	0.61
6 (n=27)	2	21 (12 – 32)	4.6
7 (ref)	1	56 (30 – 105)	1
8	7	196 (81 – 472)	0.14

[a] 95% confidence intervals are shown in brackets. Results from triplicates.

Molecular Modeling

Table 2 reports the energetic parameters (Glide energies and docking Scores) computed with Glide for altinicline derivatives **1**-**3**. We have limited the theoretical study to these first three compounds because our aim was mainly to provide a possible interpretation to the highest potency of compound **2** in terms of IC_{50}. For this investigation, we have therefore used **1** as the reference ligand and **3** as the next compound in the series.

Table 2. Relative energetic parameters (kJ/mole, using 1 as the reference compound) for the docking of altinicline derivatives **1**-**3** in the binding site of α7/Ac-AChBP.

Cpds	Energy	Score
1	0	0
2	-62.7	-0.1
3	+21.9	+0.1

The values have been calculated considering **1** as the reference compound; in other words, they correspond to relative energies (difference between energy of nicotinic derivative **2** or **3** and energy of derivative **1**). Negative values are therefore indicative of an energy stabilization in comparison with **1** whereas positive values mean destabilization of the corresponding complex. It is worth noting that 16, 8 and 4 docking poses have respectively been obtained for **1**, **2** and **3**. For the calculation of the relative energies of Table 2, we have selected the pose obtained for **1**, the closest to the experimental structure, that is to say having the closest orientation of the nicotine fragment with respect to the crystallographic structure of the nicotine-AChBP complex (1UW6). This pose

corresponds to the one ranked in ninth position (from about 16 and 2 kJ/mol in energy and score, respectively).

We were pleasantly surprised by the agreement between the docking trends and the experimental data. Thus, compound **2** appears stabilized in the binding site with respect to **1** whereas, as observed experimentally, the **3** derivative seems to have fewer interactions in the binding site. . Of course, these results have to be considered cautiously since they are limited to docking investigations but they nevertheless provide guidelines to rationalize the experimental trends. To complete this analysis, we then considered some geometric parameters of the interactions between the three nicotinic derivatives and their surroundings in the α7/*Ac*-AChBP 3D model designed. The corresponding values are reported in Supporting Information (Table S1). Figure 2 shows a global view allowing to catch the position of the binding site in α7/*Ac*-AChBP and the orientation of the three ligands.

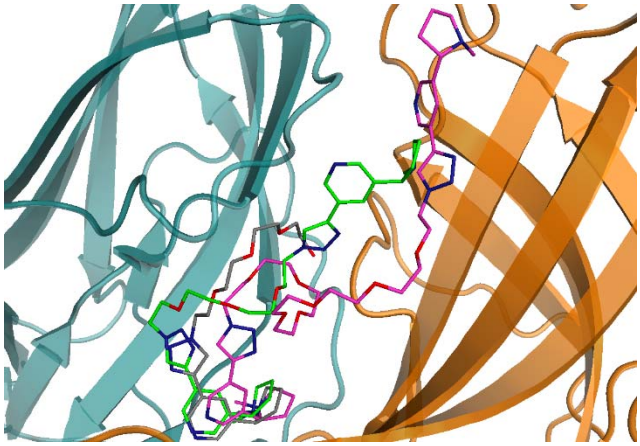

Figure 2. Global view of the orientation and position of the three altinicline derivatives (1 (grey), 2 (green), 3 (pink)) in the α7/Ac-AChBP binding site.

The orientation of the pyrrolidine ring of the nicotinic fragment of the three compounds is similar and close to the relevant nicotine–*Ac*-AChBP complex experimental structure (Figure 3). The difference of positioning becomes apparent for the **3** derivative, starting from the pyridine ring.

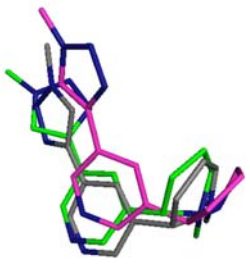

Figure 3. Detailed view of the first fragment of the three nicotinic derivatives **1** (grey), **2** (green), **3** (pink)) in the α7/Ac-AChBP binding site.

It is clear from Figure 2 that the surroundings of the nicotinic fragments are very different in derivatives **2**, **3** owing to the lengthening of the linker. It is however worth noting that the conformations adopted by the two derivatives **2** and **3** in the α7/*Ac*-AChBP environment are not extended. Figure 4 and 5 show the surroundings of the two fragments of the three derivatives, their interactions within the α7-AChBP environment being reported in Table S1 of the Supporting Information.

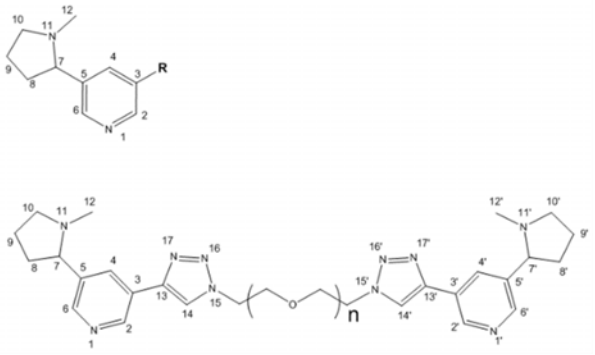

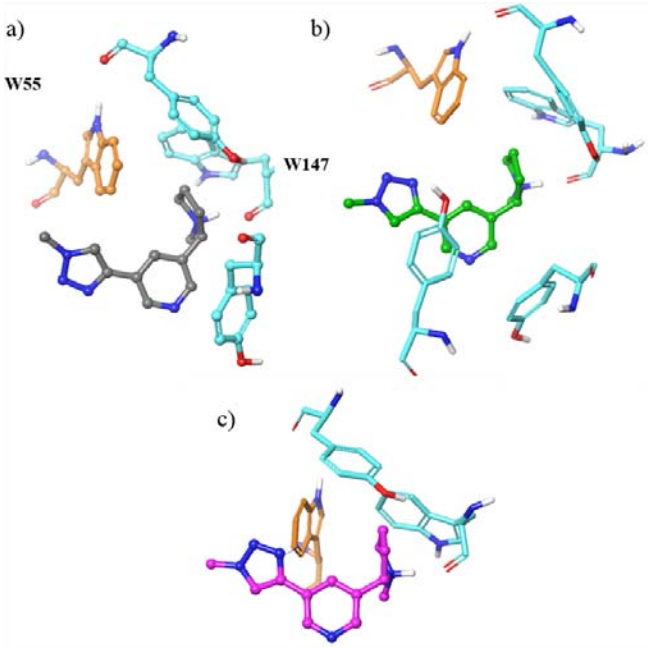

Figure 4. Environment and interactions of fragment **1** of the three altinicline derivatives: a) **1** (grey); b) **2** (green); c) **3** (pink) in the α7/*Ac*-AChBP binding site. The numbering of the key interacting amino acid residues is indicated in a) using their one letter code for better clarity (W=Trp).

Cation π interactions of the pyrrolidine ammonium moiety of nicotine with the indole ring of Trp 143, a hydrogen bond between the $N_{11}H^+$ and the main chain carbonyl of Trp 143 and an apolar contact between one carbon of the pyrrolidine ring (C9) and a carbon of the indole ring of Trp53 are key interactions of the complex between nicotine with *Ls*-AChBP in the 1UW6 crystallographic structure.[44] Table 1 and Figure 4a-c show that these contacts are conserved in the models predicted by our docking simulations for fragment 1 of the three derivatives, allowing to check the consistency of these theoretical data. Thus the π interactions between the electron deficient methylene groups of the pyrrolidine ring (C9 and C10) and the six membered ring of Trp147 are systematically obtained, as well as the key hydrogen bond interaction between the $N_{11}H^+$ ammonium group and the main chain carbonyl of Trp147. The binding pocket of fragment 1 of the three derivatives shows a significant aromatic character, several

aromatic groups of lateral chains of amino acid residues being involved in the contact with the ligands. These trends are in agreement with the known behavior of such an heteroaromatic fragment in the binding site of nAChRs. Table S1 shows that these variations of contacts for the three derivatives do not rationalize the docking energy parameters even if slight modifications are obtained.

Examination of the results predicted by the docking (Figure 5 and Table S1 in the Supporting Information) for the second fragment of the three derivatives provide guidelines to rationalize the relative stabilization of the three ligands in the α7-AChBP surroundings. Thus, it is worth noting that the ending OH group of **1** is anchored through a hydrogen bond interaction with the main chain carbonyl of Ser94 (d(O)H…O) of 1.9 Å). The greater stabilization of **2** compared to **3** can be explained by the number of contacts, which is significantly more important (4 compared to 2) and by their features. Thus, for the complex with **2**, a hydrogen bond interaction between the electron deficient C12' methyl group of the pyrrolidine ring and the main chain carbonyl of Met126 is predicted (Figure 5a) together with a cation π interaction between the ammonium group of Lys143 and the triazole ring of fragment 2. Furthermore, two additional contacts involving the pyrrolidine moiety of fragment 2 (C8' and C12') are predicted by the docking. It is interesting to note that despite the difference in length of the linker between derivatives **2** and **3**, the only amino acid residue involved in the binding of the second fragment of **3** is also involved in non-covalent interactions in **2**. As already mentioned above, this feature highlights the fact that **3** adopts a rather compact conformation in the α7-AChBP environment instead of an extended one. Figure 5, which shows the binding of the two relevant fragments of the **2** and **3** derivatives allows a better comprehension of this behavior. In fact, in **3**, the OH group of Thr139 is engaged in a hydrogen bond interaction with a nitrogen atom of the triazole ring (N17') whereas its main chain carbonyl accepts a hydrogen bond from the positively polarized C12' methyl group.

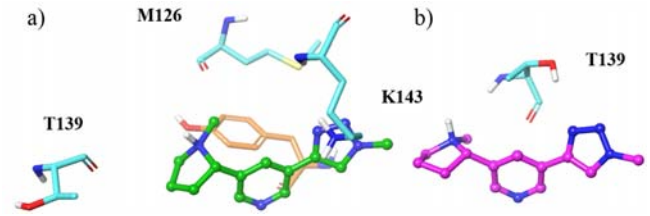

Figure 5. Environment and interactions of the fragment 2 of: a) **2** (green); b) **3** (pink)) of the nicotinic derivatives in the α7/*Ac*-AChBP binding site. The numbering of the key interacting amino acid residues is specified using their one letter code for better clarity (K=Lys; M=Met; T=Thr).

On the whole, the results of the docking simulations are in line with the experimental trends and reinforce the hypothesis according to which the variation affinity observed can be attributed to a pseudochelate effect, the second fragment of the various derivatives interacting with amino acid residues from peripheral sites.

3. Conclusion

In summary, multivalent (di- and heptavalent) nicotinic derivatives were synthesized for the first time and interesting profiles on inwards currents with α7 nAChRs were observed. The spacer arm length of divalent **2-8** was shown to significantly impact on the extent of signal inhibition. Due to the large distance between the nicotinic binding sites of α7 (around 80Å), a chelate binding mode is discarded to explain the improved inhibitory activities that should be ascribed to subsite interactions as suggested from the docking investigations. The enhanced inhibitory effect observed for **2** (n=3) remains modest compared to the improved level of inhibition observed with other channel receptors. Nevertheless, these first hints should foster nAChR subtypes evaluations of a second generation of multivalent nicotinic receptors with enhanced valency (polymers) and spacer arm length.

4. Experimental details

All reagents were purchased from Acros Organics, Alfa Aesar, or Aldrich and were used without further purification. Dichloromethane, ethyl acetate and petroleum ether were distilled on a *Buchi rotavapor R-220-SE*. Reactions requiring anhydrous conditions were performed under argon. Column chromatography was conducted on silica gel Kieselgel SI60 (40−63 μm) from Merck, or on Silica cartridge from Interchim and eluted via a Puriflash 430 with an UV and ELSD detection. Thin layer chromatography (TLC): *Merck Silica gel 60 F254* analytical plates, detection either with UV (254 nm) or dipped in a solution of potassium permanganate, ninhydrin and subsequently heated. ^{1}H and ^{13}C NMR spectra were recorded on *Bruker Avance 300* spectrometer, on a *Bruker Avance 400* spectrometer. The spectra are referenced to the solvent in which they were run. Chemical shifts (δ) are given in parts per million (ppm) and coupling constants (J) are given in Hz. Low resolution mass spectrometry (MS) was recorded on a *ThermoFinnigan DSQII quadripolar* spectrometer (coupled with a *TracUltra GC* apparatus) for Chemical Ionization (CI), on a *ThermoFinnigan LCQ Advantage* spectrometer for ElectroSpray Ionization (ESI). High resolution mass spectrometry (HRMS) was recorded on a *ThermoFisher Scientific LTQ-Orbitrap* spectrometer (for ESI+).

General method A (CuAAC). The azide derivative and the alkyne derivative (1.1 eq./azide function) were dissolved in dioxane (2mL/mmol). A solution of copper sulfate (0.2 eq./azide function) and sodium ascorbate (0.4 eq./azide function) in water (0.5mL/mmol) was added and the mixture was heated to 60°C until completion. The mixture was dissolved in DCM (50mL/mmol), washed with a solution of EDTA (50 mL/mmol) and the aqueous layer was extracted twice with DCM (2 x 50mL/mmol). The organic layer was dried over $MgSO_4$, filtered, concentrated under reduced pressure, and purified.

General method B (deprotection). The protected compound (1eq.) was dissolved in MeOH/H_2O (1:1, 1 mL/mmol). Amberlite resin IRN 78 OH- 1.25 meq/mL (150 mg/mmol) was added, and the mixture was stirred overnight at rt. The resin was filtered off and washed with methanol and water. The solvent was evaporated under reduced pressure.

Compound **1**. Obtained following the CuAAC method A. The crude product was chromatographed on a silica gel column with 9/1 (DCM/MeOH) as eluent to afford **1** (84% yield) as a white solid.

^{1}H NMR (400 MHz, D_2O): δ(ppm): 8.93 (s, 1H, H-8), 8.59 (s, 1H, H-9), 8.53 (s, 1H, H-12), 8.30 (s, 1H, H-6), 4.63 (t, J = 5.5Hz, 2H, H-14), 4.08 (t, J = 5.5Hz, 2H, H-13) (m, 1H, H-5), 3.89 (m, 1H, H-5), 3.78-3.45 (m, 13H, H-2a, CH_2O), 2.95-2.80(m, 1H, H-2b), 2.49 (bs, 4H, H-1, H-4a), 2.23-2.08 (m, 3H, H-3, H-4b); ^{13}C NMR (100 MHz, D2O): δ(ppm): 148.4 (C-8), 146.1 (C-9), 143.8 (C-11), 134.6 (C-6), 133.4, 126.7 (C-7, C-10), 123.5 (C-12), 71.8-69.3 (CH_2O), 69.0 (C-5), 68.6 (C-13), 60,3 (C-15), 56.4 (C-2), 50.4 (C-14), 38.8 (C-1), 32.1 (C-4), 21.7 (C-3); HRMS (ESI) m/z calcd for $C_{20}H_{32}N_5O_4$ [M+H+]: 406.2454, found 406.2461.

Compound **2**. Obtained following the CuAAC method A. The crude product was chromatographed on a silica gel column with 9/1 (DCM/MeOH) as eluent to afford **2** (83% yield) as a white solid.

^{1}H NMR (400 MHz, D_2O): δ(ppm): 8.67 (s, 2H, H-8), 8.56 (s, 2H, H-9), 8.33 (s, 2H, H-12), 8.13 (s, 2H, H-6), 4.61 (t, J = 5.5Hz, 4 H, H-14), 4.17-4.11 (m, 2H, H-5), 3.94 (t, J = 5.5Hz, 4 H, H-13), 3.63-3.55 (m, 9H, H-2a, CH2O), 3.16-3.07 (m, 2H, H-2b), 2.62 (s, 6H, H-1), 2.56-2.52 (m, 2H, H-4a), 2.29-2.13 (m, 6H, H-3, H-4b); ^{13}C NMR (100 MHz, D2O): δ(ppm): 148.4 (C-8), 146.3 (C-9), 143.2 (C-11), 133.0 (C-6), 132.1, 126.6 (C-7, C-10), 123.2 (C-12), 69.7-69.5 (CH2O), 69.1 (C-5), 68.5 (C-13), 56.2 (C-2), 50.3 (C-14), 38.6 (C-1), 31.3 (C-4), 21.6 (C-3); HRMS (ESI) m/z calcd for $C_{32}H_{45}N_{10}O_3$ [M+H+]: 617.3673, found 617.3677.

Compound **3**. Obtained following the CuAAC method A. The crude product was chromatographed on a silica gel column with 9/1 (DCM/MeOH) as eluent to afford 3 (91% yield) as a white solid.

^{1}H NMR (400 MHz, D_2O): δ(ppm): 8.91 (s, 2H, H-8), 8.60 (s, 2H, H-9), 8.52 (s, 2H, H-12), 8.30 (s, 2H, H-6), 4.75 (t, J = 5.4Hz, 4 H, H-14), 4.18-4.11 (m, 2H, H-5), 4.05 (t, J = 5.4Hz, 4 H, H-13), 3.78-3.62 (m, 10H, CH_2O), 3.62-3.50 (m, 15H, H-2a, CH_2O), 3.22-3.07 (m, 2H, H-2b), 2.60 (s, 6H, H-1), 2.59-2.49 (m, 2H, H-4a), 2.30-2.12 (m, 6H, H-3, H-4b); ^{13}C NMR (100 MHz, D_2O): δ(ppm): 148.3 (C-8), 146.3 (C-9), 143.3 (C-11), 133.1 (C-6), 132,5, 126.6 (C-7, C-10), 123.3 (C-12), 69.9-69.4 (CH2O), 68.9 (C-5), 68.5 (C-13), 56.1 (C-2), 50.2 (C-14), 38.4 (C-1), 31.3 (C-4), 21.5 (C-3); HRMS (ESI) m/z calcd for $C_{40}H_{60}N_{10}O_7Na$ [M+Na+]: 815.4544, found 815.4537.

Compound **4**. Obtained following the CuAAC method A. The crude product was chromatographed on a silica gel column with 9/1 (DCM/MeOH) as eluent to afford 4 (87% yield) as a white solid.

^{1}H NMR (400 MHz, D_2O): δ(ppm): 9.15 (s, 2H, H-8), 8.81 (s, 2H, H-9), 8.65-8.55 (m, 4H, H-6, H-12), 4.79 (t, J = 5.5Hz, 4 H, H-14), 4.12 (t, J = 5.5Hz, 4 H, H-13), 4.08-3.95 (m, 2H, H-5), 3.80-3.55 (m, 41H, H-2a, CH_2O), 3.55-3.40 (m, 2H, H-2b), 2.94 (s, 6H, H-1), 2.71-2.59 (m, 2H, H-4a), 2.60-2.30 (m, 6H, H-3, H-4b); ^{13}C NMR (100 MHz, D_2O): δ(ppm): 147.5 (C-8), 146.5 (C-9), 142.9 (C-11), 135.0 (C-6), 130.0, 127.9 (C-7, C-10), 124.0 (C-12), 69.9-69.2 (CH2O), 69.1 (C-5), 68.7 (C-13), 56.4 (C-2), 50.4 (C-14), 38.5 (C-1), 30.6 (C-4), 21.6 (C-3); HRMS (ESI) m/z calcd for $C_{48}H_{77}N_{10}O_{11}$ [M+H+]: 969.5773, found 969.5778.

Compound **5**. Obtained following the CuAAC method A. The crude product was chromatographed on a silica gel column with 9/1 (DCM/MeOH) as eluent to afford **5** (75% yield) as a white solid.

^{1}H NMR (400 MHz, D_2O): δ(ppm): 9.11 (s, 2H, H-8), 8.75 (s, 2H, H-9), 8.62 (s, 2H, H-12), 8.50 (s, 2H, H-6), 4.79 (t, J = 5.5Hz, 4 H, H-14), 4.11 (t, J = 5.5Hz, 4 H, H-13), 4.05-3.90 (m, 2H, H-5), 3.80-3.55 (m, 73H, H-2a, CH_2O), 3.55-3.40 (m, 2H, H-2b), 2.90 (s, 6H, H-1), 2.80-2.59 (m, 2H, H-4a), 2.60-2.32 (m, 6H, H-3, H-4b); ^{13}C NMR (100 MHz, D_2O): δ(ppm): 148.1 (C-8), 147.0 (C-9), 142.7 (C-11), 133.1 (C-6), 132.0, 128.9 (C-7), 126.5 (C-10), 123.1 (C-12), 69.2-69.1 (CH_2O, C-5), 68.0 (C-13), 55.6 (C-2), 49.8 (C-14), 37.7 (C-1), 29.7 (C-4), 20.9 (C-3); HRMS (ESI) m/z calcd for $C_{64}H_{108}N_{10}O_{19}Na$ [M+Na+]: 1343.7690, found 1343.7661.

Compound **6**. Obtained following the CuAAC method A. The crude product was chromatographed on a silica gel column with 9/1 (DCM/MeOH) as eluent to afford **6** (82% yield) as a white solid.

^{1}H NMR (400 MHz, D_2O): 9.05 (s, 2H, H-8), 8.70 (s, 2H, H-9), 8.60 (s, 2H, H-12), 8.42 (s, 2H, H-6), 4.79 (t, J = 5.5Hz, 4 H, H-14), 4.31-4.20 (m, 2H, H-5), 4.12 (t, J = 5.5Hz, 4 H, H-13), 3.82-3.52 (m, 105H, H-2a, CH2O), 3.21-3.10 (m, 2H, H-2b), 2.69 (s, 6H, H-1), 2.70-2.57 (m, 2H, H-4a), 2.40-2.20 (m, 6H, H-3, H-4b); ^{13}C NMR (100 MHz, D_2O): δ(ppm): 148.2 (C-8), 146.4 (C-9), 143.1 (C-11), 133.1 (C-6), 131.9 (C-7), 126.5 (C-10), 123.2 (C-12), 69.4-68.7 (CH_2, C-5), 68.2 (C-13), 55.8 (C-2), 49.9 (C-14), 38.1 (C-1), 30.8 (C-4), 21.4 (C-3); HRMS (ESI) m/z calcd for $C_{80}H_{141}N_{10}O_{27}$ [M+H+]: 1673.9968, found 1673.9946.

Compound **7**. Obtained following the acetate deprotection method B. The crude product was purified by size exclusion chromatography with Hitrap® column to afford **7** (96% yield) as a white solid.

^{1}H NMR (500 MHz, DMSO-d6): δ(ppm): 8.85 (s, 1H, H-8), 8.74 (s, 1H, H-9), 8.46 (s, 1H, H-12), 8.23 (s, 1H, H-6), 5.94-

5.60 (m, 13H, OH), 5.07 (d, J = 3.1Hz, 1H, H-1'), 4.98 (d, J = 13.7Hz, 1H, H-2A), 4.88-4.72 (m, 6H, H-1'), 4.68-4.59 (m, 1H, H-2B), 4.56-4.46 (m, 3H, OH), 4.09 (t, J = 9.5Hz, 1H, H-5), 3.81-3.46 (m, 21H), 3.46-3.15 (m, 44H), 2.96-2.79 (m, 2H), 2.52 (m, 3H, H-1), 2.14 (bs, 2H, H-4), 1.91 (bs, 2H, H-3); ^{13}C NMR (125 MHz, $CDCl_3$): 147.9 (C-8), 145.3 (C-9), 143.5 (C-11), 131.1 (C-6), 126.9 (C-7, C-10), 122.6 (C-12), 102.2-101.2 (C-1'), 83.5-80.7 (CH'), 73.4-71.6 (CH'), 70.1 (C-5), 67.8 (CH'), 60.5-56.3 (CH'), 50.8 (C-2), 41.2 (CH'), 35.0 (C-1), 29.0 (C-4), 22.2 (C-3); HRMS (ESI) m/z calcd for $C_{54}H_{83}N_5O_{34}$ [M+H+]: 1346.4998, found 1346.4973.

Compound **8**. Obtained following the acetate deprotection method B. The crude product was purified by size exclusion chromatography with Hitrap® column to afford **8** (96% yield) as a white solid.

^{1}H NMR (500 MHz, DMSO-d6): δ (ppm): 9.25-8.08 (m, 28H, H-6, H-8, H-9, H-12), 5.27-5.04 (m, 7H, H-1'), 4.80-4.44 (m, 14H, 2*H'), 4.44-4.15 (m, 21H, H', 14*OH), 4.10 (bs, 7H, 7*H-5), 3.74 (bs, 14H, H-2A, H'), 3.42 (bs, 7H, H'), 3.36 (bs, 7H, H'), 3.17 (bs, 7H, H-2B), 2.83-2-57 (m, 21H, H-1), 2.44-2.32 (m, 7H, H-4A), 2.27-1.92 (m, 21H, H-3, H-4B); ^{13}C NMR (125 MHz, $CDCl_3$): δ(ppm): 145.9 (C-8), 144.0 (C-9), 141.7 (C-11), 135.1 (C-6), 130.2 (C-7), 127.0 (C-10), 124.3 (C-12), 101.7 (C-1'), 82.9 (CH'), 72.3 (CH'), 71.8 (CH'), 69.4 (C-5), 68.1 (CH'), 54.8 (C-2), 49.9 (CH'), 37.3 (C-1), 31.1 (C-4), 21.0 (C-3); HRMS (ESI) m/z calcd for $C_{126}H_{164}N_{35}O_{24}$ [M+3H+]: 871.7495, found 871.7479.

Compound **17**. Obtained following the CuAAC method A. The crude product was chromatographed on a silica gel column with 9/1 (DCM/MeOH) as eluent to afford **17** (85% yield) as a white solid.

^{1}H NMR (400 MHz, $CDCl_3$): δ(ppm): 8.92 (bs, 1H, H-8), 8.45 (bs, 1H, H-9), 8.15 (bs, 1H, H-12), 7.95 (bs, 1H, H-6), 5.62 (m, 1H, H-1'), 5.40-4.90 (m, 19H), 4.85-3.95 (m, 26H), 3.80-3.50 (m, 7H), 3.33-3.05 (bs, 2H, H-2a), 2.41-1.60 (m, 66H, H-2b, H-3b, H-3a, H-4b, CH_3CO); 13C NMR (100 MHz, $CDCl_3$): δ(ppm): 170.5-169.4 (CH3CO), 148.9 (C-8), 146.1 (C-9), 144.7 (C-11), 132.1 (C-7, C-6), 126.7 (C-10), 123.6 (C-12), 97.2-96.7 (C-1'), 77.1 (C'), 70.6 (C'), 69.9 (C'), 69.2 (2xC'), 63.0-62.1 (C-6'), 57.1 (C-2), 49.4 (C'), 40.5 (C-1), 35.2 (C-4), 22.8 (C-3), 20.8 (CH_3CO); HRMS (ESI) m/z calcd for $C_{94}H_{125}N_5O_{54}$ [M+2H+]: 1093.8628, found 1093.8615.

Compound **18**. Obtained following the CuAAC method A. The crude product was chromatographed on a silica gel column with 9/1 (DCM/MeOH) as eluent to afford **1** (92% yield) as a white solid.

^{1}H NMR (400 MHz, $CDCl_3$): δ(ppm): 8.89 (bs, 7H, H-8), 8.40 (bs, 7H, H-9), 8.21 (m, 14H, H-12, H-6), 5.54 (bs, 7H, H-1'), 5.39 (bs, 7H, CH'), 5.15-4.53 (m, 28H, H-5, 3xCH'), 3.64 (bs, 7H, CH'), 3.33 (bs, 14H, H-2a, CH'), 2.41 (bs, 7H, H-2b), 2.31-2.12 (m, 28H, H-1, H-4a), 2.06 (bs, 21H, CH3CO), 1.99 (bs, 28H, CH_3CO, H-3a), 1.80-1.75 (m, 14H, H-3b, H-4b); ^{13}C NMR (100 MHz, CDCl3): δ(ppm): 170.5 (CH_3CO), 169.6 (CH_3CO), 149.0 (C-8), 146.4 (C-9), 144.6 (C-11), 133.4 (C-7), 132.3 (C-6), 126.6 (C-10), 123.9 (C-12), 96.8 (C-1'), 77.1 (CH'), 70.6 (CH'), 69.9 (C-5), 69.2 (2*CH'), 56.7 (C-2), 50.6 (CH'), 40.1 (C-1), 34.5 (C-4), 22.5 (C-3), 20.8 (CH_3CO); HRMS (ESI) m/z calcd for $C_{154}H_{191}N_{35}O_{42}$ [M+2H+]: 1601.1925, found 1601.1918.

Molecular Modeling

In the present work, the crystallographic structure of the complex between methyllycaconitine and one α7/*Ac*-AChBP (3SIO pdb entry) was used for a preliminary molecular modeling investigation of the binding characteristics of altinicline derivatives with human α7 nAChR. The crystal structure of the α7/*Ac*-AChBP complex with the methyllycaconitine antagonist (3SIO pdb entry) were downloaded from the Protein Data Bank (www.pdb.org).[45] Addition of H atoms, adjustment of ionization states of ionizable residues were carried out using the Schrödinger's protein preparation wizard. All the crystallized water molecules were kept. The 3D ligand molecules, protonated using the LigPrep v3.0 module of the Schrodinger suite 2017-1 [Schrödinger Release 2017-1, Schrödinger, LLC, New York, NY, 2014] were then subjected to the ConfGen [Schrödinger Release 2017-1: ConfGen, version 2.7, Schrödinger, LLC, New York,NY, 2017] program to retrieve the lowest energy conformer for docking. Only the "eutomer" (*S*) configuration of the nicotine-like multivalent ligands were docked, based on the configuration of nicotine in the 1UW6 crystal structure. The docking was performed using the Glide v6.3 program of the Schrodinger suite 2017-1.[46] The residues around 6˚A of the ligand were defined as the active site and were selected for the receptor grid generation. The standard-precision (SP) mode of the docking algorithm was employed to dock the altinicline derivatives. It is worth remembering that nAChRs are organized as pentamers; that is, there are five identical ligand binding sites and the ligand binds between the cleft of the two subunits. We docked the ligands in one interface (AB) of the pentameric structure, the five interfaces having close structural features.

Two-electrode voltage clamp electrophysiology on *Xenopus laevis* oocytes expressing human α7 nAChR

We purchased adult *X. laevis* females from the Biological Resource Center (University of Rennes, France). Animal care and experimental procedures were performed according to the Ethical Committee for Animal Experimentation C2EA-59 of Paris Center-South. Detailed experimental procedures for oocytes harvesting, heterologous expression of human α7 mRNA and manual two-microelectrode voltage clamp recordings (TEVC) were previously described.[47,48] For automated TEVC we used a HiClamp system (MCS GmbH., Reutlingen, Germany): single oocytes are withdrawn from the 96-wells oocyte-microplate and put it in a silver wire basket that acts also as reference bath electrode. The oocytes were automatically clamped at a holding potential of -60 mV using

glass microelectrodes (50-60 MΩ resistance) filled with a mix of 1 M KCl and 1 M ammonium acetate. The clamped oocyte was transferred into a well of the sample-microplate filled with 200 µL OR2 (88 mM Na Cl, 1 mM $MgCl_2$, 5 mM Hepes; pH 7.6) containing 100 µM acetylcholine (Ach) or the tested molecules. The amplifier allows continuous recording even during the transfer of the oocyte from the washing-station to the test-well back and forth. The micro-stirrers disposed in each test-well ensured a rapid solution exchange. Dose-response curves for agonist activation were analyzed using the equation:

$I = I_{max}[L]^{nH}/(EC_{50} + [L])^{nH}$, where I is the measured agonist-evoked current, [L] is the agonist concentration, EC_{50} is the agonist concentration that evoked half the maximal current (I_{max}), and nH is the Hill coefficient. For antagonist inhibition, current (I) values were normalized to the I_{max} value recorded from the same oocyte to yield fractional (%) response data. IC_{50} values were determined from dose-response curves by fitting to the equation: $F = 1/[1 + ([X]/IC_{50})^{nH}]$, where F is the fractional response obtained in the presence of the inhibitor at concentration [X] and IC_{50} is the inhibitor concentration that reduced the ACh-evoked amplitude by half.

Acknowledgments

This work was carried out with financial support from the Conseil Régional des Pays de La Loire (MAGGIC project), the Centre National de la Recherche Scientifique (CNRS) and the Ministère de l'Enseignement Supérieur et de la Recherche in France.

Supplementary Material

Supplementary data associated with this article can be found, in the online version.

References and notes

1. Cecioni S, Imberty A, Vidal S. *Chem Rev*. 2015;115:525.
2. Wittmann V, Pieters RJ. *Chem Soc Rev*. 2013;42:4492.
3. Gouin SG. *Chem – Eur J*. 2014;20:11616.
4. Compain P, Bodlenner A. *ChemBioChem*. 2014;15:1239.
5. Matassini C, Parmeggiani C, Cardona F, Goti A. *Tetrahedron Lett*. 2016;57:5407.
6. Kanfar N, Bartolami E, Zelli R, et al. *Org Biomol Chem*. 2015;13:9894-9906.
7. Mellet CO, Nierengarten J-F, Fernández JMG. *J Mater Chem B*. 2017;5:6428.
8. Abellán Flos M, García Moreno MI, Ortiz Mellet C, García Fernández JM, Nierengarten J-F, Vincent SP. *Chem – Eur J*. 2016;22:11450.
9. García-Moreno MI, Ortega-Caballero F, Rísquez-Cuadro R, Ortiz Mellet C, Fernandez G, M J. *Chem - Eur J*. 2017;23,6295.
10. Thobhani S, Ember B, Siriwardena A, Boons G-J. *J Am Chem Soc*. 2003;125:7154.
11. Brissonnet Y, Ortiz Mellet C, Morandat S, et al. *J Am Chem Soc*. 2013;135:18427.
12. Howard E, Cousido-Siah A, Lepage ML, et al. *Angew Chem Int Ed*. 2018;57:8002.
13. Bernardi A, Jimenez-Barbero J, Casnati A, et al. *Chem Soc Rev*. 2013;42,4709.
14. Deniaud D, Julienne K, Gouin SG. *Org Biomol Chem*. 2011;9:966.
15. Kopinathan A, Scammells PJ, Lane JR, Capuano B. *Future Med Chem*. 2016;8:1349.
16. Pang Y-P, Quiram P, Jelacic T, Hong F, Brimijoin S. *J Biol Chem*. 1996;271:23646.
17. Kanfar N, Tanc M, Dumy P, Supuran C, Ulrich S, Winum J-Y. *Chem – Eur J*. 2017;23:6788.
18. Busnelli M, Kleinau G, Muttenthaler M, et al. *J Med Chem*. 2016;59:7152.
19. Antony J, Kellershohn K, Mohr-Andrä M, et al. *FASEB J*. 2009;23:442.
20. Maric HM, Kasaragod VB, Schindelin H. *ACS Chem Biol*. 2014;9:2554.
21. Kramer RH, Karpen JW. *Nature*. 1998;395:710.
22. Paolino M, Mennuni L, Giuliani G, et al. *Chem Commun*. 2014;50:8582.
23. Umana IC, Daniele CA, McGehee DS. *Biochem Pharmacol*. 2013;86:1208.
24. Taly A, Corringer P-J, Guedin D, Lestage P, Changeux J-P. *Nat Rev Drug Discov*. 2009;8:733.
25. Romanelli MN, Gratteri P, Guandalini L, Martini E, Bonaccini C, Gualtieri F. *ChemMedChem*. 2007;2:746.
26. Katju&Sbreve, Brejc A, van Dijk WJ, et al. *Nature*. 2001;411:269.
27. Nemecz Á, Taylor P. *J Biol Chem*. 2011;286:42555.
28. Li S-X, Huang S, Bren N, et al. *Nat Neurosci*. 2011;14:1253.
29. Scates BA, Lashbrook BL, Chastain BC, et al. *Bioorg Med Chem*. 2008;16:10295.
30. Chen D, Patrick JW. *J Biol Chem*. 1997;272:24024.
31. Cosford NDP, Bleicher L, Herbaut A, et al. *J Med Chem*. 1996;39:3235.
32. Prime KL, Whitesides GM. *Science*. 1991;252:1164.
33. Krishnamurthy VM, Semetey V, Bracher PJ, Shen N, Whitesides GM. *J Am Chem Soc*. 2007;129:1312.
34. Bouckaert J, Li Z, Xavier C, et al. *Chem – Eur J*. 2013;19:7847.
35. Ulens C, Akdemir A, Jongejan A, et al. *J Med Chem*. 2009;52:2372.
36. Fan E, Zhang Z, Minke WE, Hou Z, Verlinde CLMJ, Hol WGJ. *J Am Chem Soc*. 2000;122:2663.
37. Dam TK, Gerken TA, Cavada BS, Nascimento KS, Moura TR, Brewer CF. *J Biol Chem*. 2007;282:28256.
38. Sacchettini JC, Baum LG, Brewer CF. *Biochemistry*. 2001;40:3009.
39. Bakleh ME, Sol V, Estieu-Gionnet K, Granet R, Déléris G, Krausz P. *Tetrahedron*. 2009;65:7385.
40. Lehot V, Brissonnet Y, Dussouy C, et al. *Chem – Eur J*. 2018;24:19243.
41. Schaschke N, Musiol H-J, Assfalg-Machleidt I, Machleidt W, Rudolph-Böhner S, Moroder L. *FEBS Lett*. 1996;391:297.
42. Boger J, Corcoran RJ, Lehn J-M. *Helv Chim Acta*. 1978;61:2190.
43. Rodios NA. *J Heterocycl Chem*. 1984;21:1169.
44. Celie PHN, Rossum-Fikkert SE van, Dijk WJ van, Brejc K, Smit AB, Sixma TK. *Neuron*. 2004;41:907.
45. Berman HM, Battistuz T, Bhat TN, et al. 2002;58:899.
46. Friesner RA, Banks JL, Murphy RB, et al. *J Med Chem*. 2004;47:1739.
47. Araoz R, Servent D, Molgó J, et al. *J Am Chem Soc*. 2011;133:10499.
48. Aráoz R, Ouanounou G, Iorga BI, et al. *Toxicol Sci*. 2015;147:156.